Scaling of Driven Magnetic Reconnection Rates

A. Y. Aydemir and A. B. Gott

Institute for Fusion Studies

The University of Texas at Austin

Austin, TX 78712 USA

(Dated: December 16, 2003)

Abstract

Computational experiments in various collisionality regimes show that, when the drive is unambiguously separated from the reconnection region, driven magnetic reconnection, in its idealized and extensively studied two dimensional form, proceeds at a rate determined only by the boundary conditions. Within certain bounds, details of the physics model used in studying this ubiquitous phenomenon play only a peripheral role: they determine the structure of the reconnection layer but not the overall reconnection rate. Therefore, scaling laws for models where this separation is absent will tend to be problem specific features, not universal laws of driven magnetic reconnection.

PACS numbers: 52.30.Ex, 52.35.Vd, 52.65.Kj

Magnetic reconnection changes the topology of magnetic fields embedded in highly conducting plasmas, while at the same time converting some of the stored energy in the field into kinetic and internal energies of the plasma. It has been studied extensively in laboratory, geophysical, and astrophysical contexts and is now the subject of entire monographs[1, 2]. Although early discussions were carried out mainly in terms of resistive (collisional) magnetohyrodynamic (MHD) models, more recent works have focused on the role of collisionless and related physics brought in by extensions of resistive MHD. Some of the recent advances are discussed by Biskamp *et al.*[3], and Bhattacharjee *et al.*[4].

From the very beginning, the rate of reconnection has been the crucial question, and various answers, based mostly on phenomenological arguments, have been proposed. Of these, the best known are the Sweet-Parker current sheet model[5, 6], which predicts a rate that scales as $\eta^{1/2}$, where η is a measure of the resistivity in the reconnection layer, and the Petschek model[7], which predicts a much weaker, logarithmic, dependence on resistivity. The former is usually considered to be too slow, especially to explain the energetics of solar flares, its original goal, and the latter is considered unphysical, since it ignores the essential physics of the diffusion layer. Despite decades of research, this topic is still a source of controversy and misunderstanding, and the goal of this article is to provide a definitive answer in a somewhat narrow but well-defined context.

A physical system in which magnetic field lines go through a topology change can be conceptually divided into two sections: an inner "reconnection region" that includes the reconnection layer (where the ideal MHD assumption breaks down) and its immediate surroundings, and an outer region that provides the drive for reconnection, a source of mechanical or potential energy. In this sense, reconnection is always a driven process, and the rate of reconnection is a function, not only of the physics of the inner region, but also of the strength of the drive that originates outside. Thus, limits on reconnection rates can only be studied accurately in cases where this conceptual division is also introduced physically, separating and isolating the driver from the driven inner section.

An example of an unambiguously driven physical system is the Versatile Toroidal Facil-

ity (VTF) experiment[8], where reconnection is driven by an externally generated inductive electric field in a separately produced quadrupolar cusp field. Our goal here is to study magnetic reconnection numerically in a similar system, but in two dimensions. The quadrupole field geometry used in our studies is shown in Fig. 1.

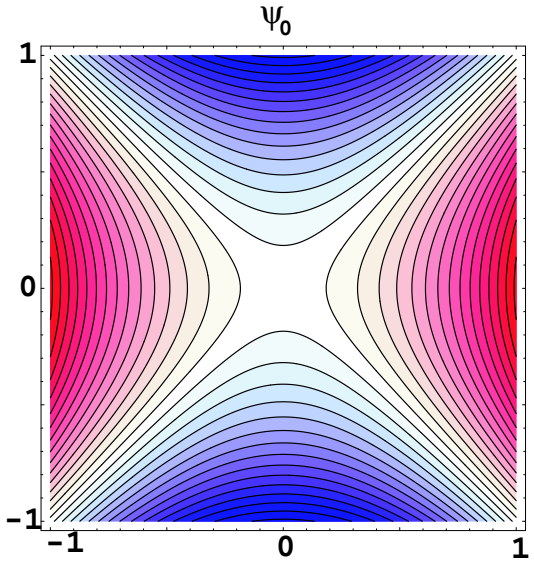

FIG. 1: Initial quadrupolar field geometry with a center X-point used in the numerical studies.

For our work we use a number of different but related models to describe the reconnection dynamics in various collisionality regimes. The first is a reduced two-fluid model that retains the electron inertia and electron pressure terms in a generalized Ohm's law. It has been discussed extensively in the literature[9] and is presented here without discussion:

$$\frac{dU}{dt} = [J,\psi] + \mu\nabla_\perp^2 U, \tag{1}$$

$$\frac{dF}{dt} = \rho_s^2[U,\psi] + \eta\nabla_\perp^2\psi - \nu\nabla_\perp^4\psi, \tag{2}$$

The magnetic field is of the form $\boldsymbol{B} = B_z\boldsymbol{e}_z + \nabla\psi\times\boldsymbol{e}_z$, where B_z is a strong "guide field" in the symmetry direction $\boldsymbol{e}_z$. The fluid velocity is given by $\boldsymbol{v} = \boldsymbol{e}_z\times\nabla\phi$, and the Poisson brackets are defined by $[A,B] = \boldsymbol{e}_z\cdot\nabla A\times\nabla B$. For any scalar A, we define $dA/dt \equiv \partial A/\partial t + [\phi, A]$. The fluid vorticity is given by $U = \nabla^2\phi$, and the current density is $J = -\nabla^2\psi$. The generalized flux function $F \equiv \psi + d_e^2 J$ represents the axial component of the canonical momentum. The electron skin depth is $d_e = c/\omega_{pe}$, and $\rho_s = \sqrt{T_e/m_i}/\omega_{ci}$

is the ion sound length, or the ion gyroradius at the electron temperature. The lengths are normalized to a typical system size $L \equiv L_x = L_y$, and times are given in units of the Alfvén time $\tau_A = L/v_A$, where $v_A = B_\infty/\sqrt{\mu_0 \rho}$. Quantities of the form B_∞ refer to values at the computational boundary. The viscosity (μ) and hyper-resistivity (ν) terms are included for numerical reasons. Note that by letting $d_e = \rho_s = 0$ in Eq. 2, we obtain the usual 2D reduced, resistive MHD model, used in our purely resistive calculations.

The second model is a Hall MHD system that ignores electron inertia and pressure terms ($d_e = \rho_s = 0$) in the generalized Ohm's law but adds the ion skin-depth length scale $d_i = c/\omega_{pi}$. It also removes the strong guide field assumption while still maintaining incompressibility. The particular form of the equations given below is due to Fitzpatrick[10], with a slightly different sign convention:

$$\frac{dU}{dt} = [J, \psi] + \mu \nabla_\perp^2 U, \tag{3}$$

$$\frac{d\psi}{dt} = d_i [\psi, B_z] + \eta \nabla_\perp^2 \psi - \nu \nabla_\perp^4 \psi, \tag{4}$$

$$\frac{dV_z}{dt} = [B_z, \psi] + \mu \nabla_\perp^2 V_z, \tag{5}$$

$$\frac{dB_z}{dt} = [V_z, \psi] + d_i [\psi, J] + \mu \nabla_\perp^2 B_z - \nu \nabla_\perp^4 B_z, \tag{6}$$

where now $\boldsymbol{v} = \boldsymbol{e}_z \times \nabla \phi + \boldsymbol{e}_z V_z$.

For all our calculations, the initial conditions are the same as those used by Ramos *et al.*[11] in their initial-value study of reconnection in VTF, except for a rotation of the fields by $\pi/4$ to align the generated current sheets with one of the coordinate directions: $\psi_0(x, y) = (B_\infty/2)(y^2 - x^2)$, and $\phi_0(x, y) = E_\infty/(4B_\infty) \ln\left((y^2 + x^2) + \delta^2)/((y^2 - x^2) + \delta^2)\right)$, where δ is a regularizing parameter chosen to be larger than other relevant length scales. The (quasi)steady-state results are independent of the exact functional dependence of ϕ_0 and ψ_0 on δ, or on its exact value. In the Hall MHD model, we let $B_{z0}(x, y) = V_{z0}(x, y) = 0$. For computational reasons, the fields are written in the form $\psi(x, y, t) = \psi_0(x, y) + \tilde{\psi}(x, y, t)$, etc., with no assumptions on the magnitude of $\tilde{\psi}/\psi_0$. The boundary conditions for the time-varying components are: $\tilde{\phi} = \tilde{U} = \tilde{B}_z = 0$, and $\partial\tilde{\psi}/\partial n = \partial\tilde{F}/\partial n = \partial\tilde{J}/\partial n = \partial\tilde{V}_z/\partial n = 0$, where n represents the normal direction to the boundary. Note that for our purposes, the

relevant difference between the two models above is that in the reduced two-fluid equations (Eqs. (1-2)), the small-scale dynamics is controlled by kinetic Aflvén waves, driven by the ρ_s-term in the Ohm's law, whereas in the HMHD model, this role is played by the whistler waves due to d_i-terms[12].

The main result of this work, the linear dependence of the reconnection rate on the external electric field E_∞, is shown in Fig. 2, where we plot the reconnection rate as a function of the applied electric field E_∞ for $10^{-3} \leq E_\infty \leq 0.6$. The data was produced by incrementally increasing E_∞ after a (quasi)steady-state was reached at the previous value (an example is shown later in Fig. 4). The rate is measured by the electric field at the X-point, calculated as $E_X \equiv -\partial\psi(x=0,y=0,t)/\partial t$. The plot shows results from all three of the physics models mentioned above: the purely resistive case, the reduced two-fluid model, and the Hall MHD model. With some small variations, all three models exhibit the simple scaling law, $E_X \simeq E_\infty$: The reconnection rate is determined by the external drive, regardless of the reconnection layer physics. This result precludes spurious scaling of E_X with other parameters, as sometimes reported in the literature; within practical computational limits, it holds independently of the values chosen for various parameters such as d_e, d_i, ρ_s, and η. Thus, in *truly driven* reconnection, the only relevant parameter is the strength of the drive, and the dependence of E_X on any other variable seen in other contexts has to be attributed to an interaction of the reconnection region, as defined above in the introduction, with the region driving the reconnection, i.e, a lack of clear separation of the drive from the driven. Since this interaction is usually a complicated function of the geometry and details of the physics model, it is only natural that each model without this separation will lead to a different scaling of the reconnection rate with the applicable parameters. But any such scaling "law" cannot be general, and the only general scaling law in driven reconnection is $E_X \simeq E_\infty$.

Unfortunately, in most driven reconnection studies in the literature, this clear separation is missing. Thus, the results quoted can only be problem dependent. In particular, the peak reconnection rate of $E \sim 0.24 B_0 v_A$ quoted by the GEM Challange work [13] for the

Harris pinch problem and other similar claims[14] cannot be "universal". Similarly, it is not meaningful to discuss the differences in reconnection rate scalings when the model problems themselves are different, as in the differences, for example, between the Harris pinch results of Wang *et al.*[15] and the results of Fitzpatrick for the Taylor problem[10].

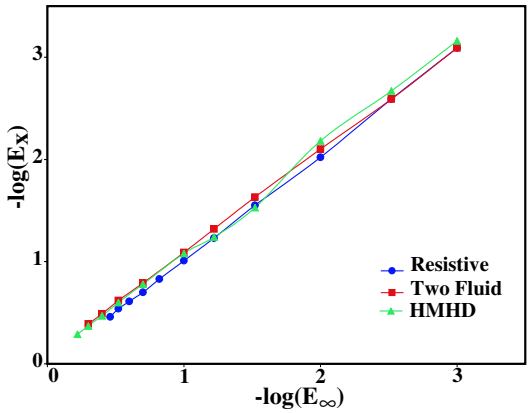

FIG. 2: Reconnection rate as a function of the applied electric field. Purely resistive: $d_e = \rho_s = d_i = 0, \eta = 10^{-3}$. Reduced two-fluid model: $d_e = 0.1, \rho_s = 0.2, \eta = 10^{-3}$. Hall MHD model: $d_i = 0.2, \eta = 10^{-3}$.

Although all three physics models exhibit the simple scaling of the reconnection rate with the applied electric field, $E_X \simeq E_\infty$, details, in particular those of the current sheets, differ markedly between the purely resistive model and the semi-collisional/collisionless models. In the collisional case, where we used $\eta = 10^{-3}, L = 1.5, B_\infty = 1.5$, the well-known Sweet-Parker rate is $M_{SP} = (\eta/Lv_{A\infty})^{1/2} = 2.1 \times 10^{-2}$. For $E_\infty < E_{SP} \equiv M_{SP}[v_{A\infty}B_\infty] = 4.7 \times 10^{-2}$, reconnection proceeds without modifying the $X-$point geometry of the initial quadrupole field. For $E_\infty > E_{SP}$, however, the flux arrives at the layer faster than the rate of dissipation, and we enter the flux pile-up regime[16], leading to an elongated current sheet, as extensively discussed by Biskamp[17]. Figure 3(a) shows the highly extended structure of the current layer for $E_\infty = 0.35$. The inflow velocity and field amplitude at the edge of the resistive layer are $v_{in} \simeq 0.1$, $B_{in} \simeq 4.$, as seen in panels (b) and (c) of Fig. 3. Unlike the usual Sweet-Parker model, these values are quite different from the asymptotic values at the boundary, $B_\infty = 1.5$, and $u_\infty = E_\infty/B_\infty = 0.23$. Note also that the outflow from the layer is nearly Alfvénic, with a peak velocity of $v_{max} \simeq 1.9$, which is approximately 2/3 of the Alfvén speed at the edge of the layer. The electric field is uniform, $E_\infty = u_\infty B_\infty \simeq v_{in}B_{in} \simeq E_X$,

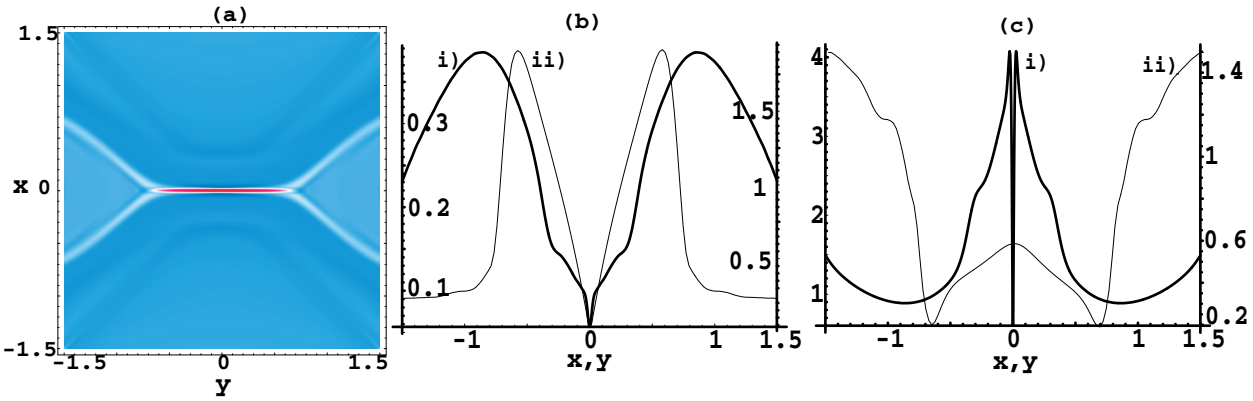

FIG. 3: Global structure of the reconnection layer in the purely resistive case for $E_\infty = 0.35$, and $\eta = 10^{-3}$. a) The current sheet, b) Profiles of the inflow and outflow velocities. i) Inflow, $|v(x, y = 0)|$ (left vertical scale), ii) Outflow, $|v(x = 0, y)|$ (right vertical scale). c) Profiles of the magnetic field amplitude. i) $|B(x, y = 0)|$, ii) $|B(x = 0, y)|$. Note that all variables in the calculations are "cell-centered", thus the values shown are actually from $x = \Delta x/2$ instead of $x = 0$ (similarly for y).

and within the layer, it is balanced by the resistive term: $E_X \simeq \eta J_X$. Note that in a self-consistent (self-contained) problem, such as the evolution of the $m = 1$ internal kink mode in tokamaks, the flux pile-up observed here [Fig. 3(c)] would immediately start reducing the potential energy available to the mode, *i.e.* slow down the drive, so that the nonlinear mode evolves at the Sweet-Parker rate[18].

For $E_\infty \geq 0.35$, the extended current sheet eventually breaks up due to a tearing instability, which leads to a series of intermittent reconnection events[17]. Reconnection rate in this regime becomes hard to quantify and is not examined further in this Letter. Note that this limit, $E_\infty = 0.35$, is not universal but depends on various other parameters in the problem.

Reconnection in the resistive regime is generally termed "slow", since, as we saw above, the inflow Mach number $M_{in} \equiv u_{in}/B_{in} \sim M_{SP}$. We note, however, the actual reconnection rate is given by $E_X \simeq E_\infty$, and in this sense, there is really nothing slow about resistive reconnection. Clearly, a strong drive coupled with small resistivity may lead to an extreme regime where $B_{in}/B_\infty \gg 1$. However, a discussion of at what value of E_∞ the resulting pile-up regime becomes unphysical is beyond the scope of this paper; the important point is that within the context of this extensively studied model, the rate is determined by the boundary conditions, until the layer becomes unstable to secondary tearing modes.

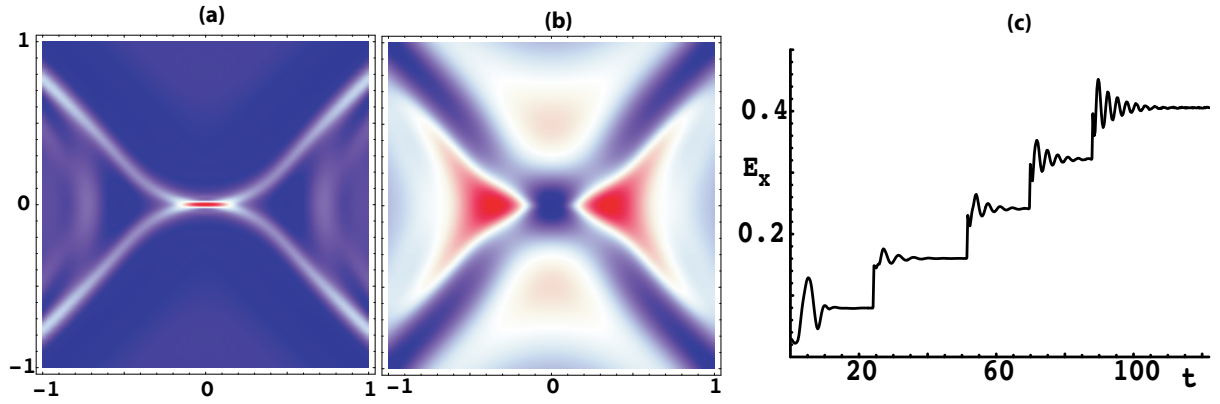

FIG. 4: a) The current sheet in the two-fluid model, for $E_\infty = 0.40,\ d_e = 0.1,$ and $\rho_s = 0.2$. b) $v^2 = |\nabla\phi|^2$. c) A partial time history of the electric field at the $X-$point.

The observation $E_X \simeq E_\infty$ is easier to establish in the semi-collisional/collisionless regimes using the reduced two-fluid or Hall-MHD models, where the currents are mostly localized around the $X-$point, and the numerical challenges associated with an extended current sheet do not arise. For the reduced two-fluid model, geometry of the reconnection layer is shown in Fig. 4 for $E_\infty = 0.4$. We note that, even with these strong drives ($M_\infty \equiv u_\infty/v_{A\infty} = 0.4$), the layer essentially maintains the $X-$point geometry of the initial field. The outflow from the layer is through wide-open "nozzles" [Fig. 4(b), the red-colored regions], as first reported for a cylindrical $m = 1$ mode in tokamaks using a similar physics model[19]. We have been able to drive this system up to $E_\infty = 0.5$ ($M_\infty = 0.5$), beyond which poorly understood, large-amplitude oscillations in time corrupt the numerical results. A partial time history of the electric field at the $X-$point, as it responds to incremental changes to the field at the boundary, is shown in Fig. 4(c).

The Hall-MHD model calculations, despite the differences in physics governing the small-scale dynamics (whistlers here vs. the kinetic Alfvén waves above), produce results similar to those obtained with the reduced two-fluid model. Figure 5 shows the global structure in the Hall-MHD layer for $E_\infty = 0.4$. The current layer is again localized around the $X-$point. The contours of the out-of-plane B_z field, due to whistlers and presumably responsible for maintaining the $X-$point structure of the layer[12], are shown in Fig. 5(b). Interestingly, the outflow from the layer has the form of two well-collimated jets here [Fig. 5(c)], which

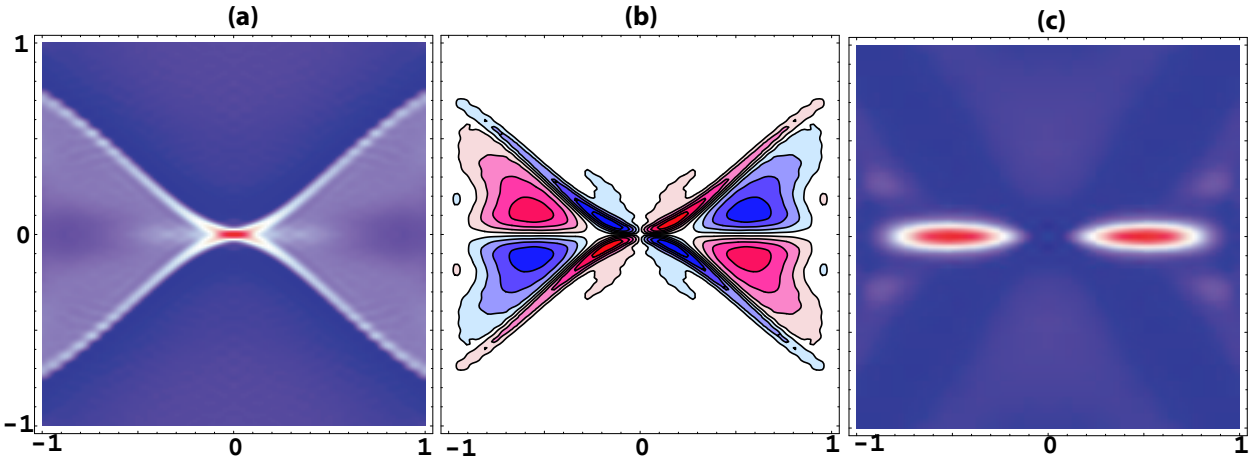

FIG. 5: Global structure of layer in the Hall-MHD model, for $E_\infty = 0.40$ and $d_i = 0.2$. a) The current sheet, b) Contours of B_z, the out-of-plane component of the field, c) $v^2 = |\nabla\phi|^2$.

differs from the flow in two fluid model above [Fig. 4(b)], where it fans out following the contours of the opening separatrix. Note also that the two maxima in v^2 are located well-outside the layer. This series of calculations were stopped at $E_\infty = M_\infty = 0.6$ because of time constraints. We have not yet seen any physical or numerical limits to how hard this system can be driven.

As stated earlier, in the resistive calculations, the (quasi)steady-state current density in the layer is such that the electric field is balanced by the resistive term in the Ohm's law: $E_X \simeq \eta J_X$. For the reduced two-fluid and Hall-MHD calculations, with similar spatial resolutions, the observed current density amplitude is at least an order of magnitude lower and $E_X \gg \eta J_X$. (The resistivity for all three series of calculations was fixed at $\eta = 10^{-3}$.) In the two-fluid model, the electron inertia terms lead to a well-known, cusp-like structure in J_z at the $X-$point that cannot be fully resolved numerically - effective dissipation level is set by numerics or the hyper-resistivity term. In the HMHD model, again there appears to be good physical reasons why the resistive term can never balance the electric field at the $X-$point[20], and one has to invoke at least a fourth-order dissipation term (hyper-resistivity) to balance the reconnection field: $E_X \sim \nu\nabla_\perp^4\psi$.These observations might explain the experimental results from VTF, where they report very little current, or equivalently, a very high anomalous resistivity, around the $X-$point in the collisionless regime[8]. Of

course, there may be other reasons, such as the effects of the off-diagonal terms in the pressure tensor[21], which we plan to examine in a separate work.

In summary, in driven reconnection where the drive is separated unambiguously from the reconnection region, the rate is determined by the boundary conditions, i.e., by the strength of the drive. Details of the physics model used in the reconnection region only determine the structure of the layer but not the rate of reconnection. Thus, truly driven reconnection has only one scaling law: $E_X \simeq E_\infty$. Without this clear separation, the driven-reconnection scaling "laws" found in various problems will tend to be context-dependent and not universal.

This work was supported by the U.S. DoE under grant No. DE-FG03-96ER-54346. Computational resources were provided by the National Energy Research Scientific Computing Center, supported by the U.S. DoE under Contract No. DE-AC03-76SF00098.

[1] Dieter Biskamp. *Magnetic Reconnection in Plasmas*. Cambridge University Press, 2000.

[2] Eric Priest and Terry Forbes. *Magnetic Reconnection, MHD Theory and Applications*. Cambridge University Press, 2000.

[3] D. Biskamp, E. Schwarz, and J. F. Drake. Phys. Plasmas, **4**, 1002 (1997).

[4] A. Bhattacharjee, Z. W. Ma, and Xiaogang Wang. Phys. Plasmas, **8**, 1829 (2001).

[5] P. A. Sweet. Nuovo Cimento Suppl., **8** 188 (1958).

[6] E. N. Parker. J. Geophys. Res. **62**, 509 (1957).

[7] H. E. Petschek. In *AAS/NASA Symposium on the Physics of Solar Flares*, page 425, Washington, 1964. NASA.

[8] J. Egedal, A. Fasoli, D. Tarkowski, and A. Scarabosio. Phys. Plasmas, **8**, 1935 (2001).

[9] T. J. Schep, F. Pegoraro, and B. N. Kuvshinov. Phys. Plasmas, **1**, 2843 (1994).

[10] R. Fitzpatrick. Submitted to Phys. Plasmas, (2003).

[11] J. J. Ramos, F. Porcelli, and R. Verástegui. Phys. Rev. Lett., **89**, 055002 (2002).

[12] B. N. Rogers, R. E. Denton, J. F. Drake, and M. A. Shay. Phys. Rev. Lett, **87**, 195004 (2001).

[13] J. Birn, J. F. Drake, M. A. Shay, B. N. Rogers, and R. E. Denton, M. Hesse, M. Kuznetsova,

Z. W. Ma, A. Bhattacharjee, A. Otto, and P. L. Pritchett. J. Geophys. Res., **106**, 3715 (2001).

[14] D. Biskamp, E. Schwartz, and J. F. Drake. Phys. Rev. Lett., **75**, 3850 (1995).

[15] X. Wang, A. Bhattacharjee, and Z. W. Ma. Phys. Rev. Lett., **87**, 265003 (1995).

[16] E. R. Priest. Geophys. Monogr., Am. Geophys. Union, **30**, 63 (1984).

[17] D. Biskamp. Phys. Fluids , **29**, 1520 (1986).

[18] A. Y. Aydemir, J. C. Wiley, and D. W. Ross, Phys. Fluids B, **1**, 774 (1989).

[19] A. Y. Aydemir. Phys. Fluids B, **4**, 3469 (1992).

[20] M. A. Shay, J. F. Drake, B. N. Rogers, and R. E. Denton. J. Geophys. Res., **106**, 3759 (2001).

[21] J. J. Ramos. Personal communication (2003).

Fig. 1: Initial quadrupolar field geometry with a center X-point used in the numerical studies.

Fig. 2: Reconnection rate as a function of the applied electric field. Purely resistive: $d_e = \rho_s = d_i = 0, \eta = 10^{-3}$. Reduced two-fluid model: $d_e = 0.1, \rho_s = 0.2, \eta = 10^{-3}$. Hall MHD model: $d_i = 0.2, \eta = 10^{-3}$.

Fig. 3: Global structure of the reconnection layer in the purely resistive case for $E_\infty = 0.35,$ and $\eta = 10^{-3}$. a) The current sheet, b) Profiles of the inflow and outflow velocities. i) Inflow, $|v(x, y = 0)|$ (left vertical scale), ii) Outflow, $|v(x = 0, y)|$ (right vertical scale). c) Profiles of the magnetic field amplitude. i) $|B(x, y = 0)|$, ii) $|B(x = 0, y)|$. Note that all variables in the calculations are "cell-centered", thus the values shown are actually from $x = \Delta x/2$ instead of $x = 0$ (similarly for y).

Fig. 4: a) The current sheet in the two-fluid model, for $E_\infty = 0.40,$ $d_e = 0.1,$ and $\rho_s = 0.2$. b) $v^2 = |\nabla\phi|^2$. c) A partial time history of the electric field at the $X-$point.

Fig. 5: Global structure of layer in the Hall-MHD model, for $E_\infty = 0.40$ and $d_i = 0.2$. a) The current sheet, b) Contours of B_z, the out-of-plane component of the field, c) $v^2 = |\nabla\phi|^2$.